Mutations at the Alphavirus E2/E1 inter-dimer interface have host-specific phenotypes

Sophia C. Ren[1,±], Shefah A. Qazi[1,±], Brian Towell[2], Joseph CY Wang[3], and Suchetana Mukhopadhyay[1,*]

[1]Department of Biology, [2]Molecular and Cellular Biochemistry, Indiana University, Bloomington, IN 47405, and [3]Department of Microbiology and Immunology, Penn State College of Medicine, Hershey, PA 17033

Running Title: Contacts between E1-E2 heterodimers affect particle assembly

[±]These authors contributed equally to this work
[2]Current address: LabCorp Drug Development. Indianapolis, IN

*Corresponding author: 212 S. Hawthorne Drive, Bloomington, IN 47405.
812-856-3686 (Phone)
sumukhop@indiana.edu (Email)

ABSTRACT

Alphaviruses are enveloped viruses transmitted by arthropod vectors to vertebrate hosts. The surface of the virion contains 80 glycoprotein spikes embedded in the membrane and these spikes mediate attachment to the host cell and initiate viral fusion. Each spike consists of a trimer of E2-E1 heterodimers. These heterodimers interact at two interfaces: (1) the intra-dimer interactions between E2 and E1 of the same heterodimer, and (2) the inter-dimer interactions between E2 of one heterodimer and E1 of the adjacent heterodimer (E1'). We hypothesized that the inter-dimer interactions are essential for trimerization of the E2-E1 heterodimers into a functional spike. In this work, we made a mutant virus (CPB) where we replaced six inter-dimeric residues in the E2 protein of Sindbis virus (WT SINV) with those from the E2 protein from chikungunya virus, and studied its effect in both mammalian and mosquito cell lines. CPB produced fewer infectious particles in mammalian cells than in mosquito cells, relative to WT SINV. When CPB virus was purified from mammalian cells, particles showed reduced amounts of glycoproteins relative to capsid protein, and contained defects in particle morphology compared to virus derived from mosquito cells. Using cryo-EM, we determined that the spikes of CPB had a different conformation than WT SINV. Last, we identified two revertants, E2-H333N and E1-S247L, that restored particle growth and assembly to different degrees. We conclude the inter-dimer interface is critical for spike trimerization and is a novel target for potential antiviral drug design.

IMPORTANCE

Alphaviruses, which can cause disease when spread to humans by mosquitoes, have been classified as an emerging pathogen, with infections occurring worldwide. The spikes on the surface of the alphavirus particle are absolutely required for the virus to enter a new host cell and initiate an infection. Using a structure-guided approach, we made a mutant virus that alters spike assembly in mammalian cells but not mosquito cells. This is important because it identifies a region in the spike that could be a target for antiviral drug design.

INTRODUCTION

Alphaviruses are most commonly transmitted by arthropod vectors, usually mosquitoes, to vertebrate hosts, including humans, birds, and horses (1, 2). While a majority of alphaviruses have an arthropod vector, a group of alphaviruses have been identified to transmit only between invertebrates (3), and others use a different vector to infect aquatic animals (4). Therefore, for an alphavirus to complete its infection cycle, it must be able to assemble particles in all of these host environments. Virus infection must rely on different host factors since the same viral proteins are synthesized.

The alphavirus genome consists of four nonstructural proteins and six structural proteins, which are required for viral genome replication and particle assembly, respectively (1, 2, 5, 6). The alphavirus particle consists of an inner nucleocapsid core, a host-derived lipid membrane, and 80 trimeric spikes on the surface of the virion (7). The spikes are trimers of E2-E1 heterodimers with each heterodimer forming the edge of a triangular spike. Both the E2 and E1 proteins each contain a single transmembrane domain and are embedded within the viral membrane. The endodomain of E2 interacts with the capsid protein in the core in a 1:1 ratio (8-12). Thus, the E2 protein transits the entire particle and helps align the core and the spikes, a unique feature of alphaviruses compared to other enveloped viruses (7).

Alphavirus spike assembly is a highly regulated process that depends on specific interactions between the viral proteins and host factors. The structural proteins are translated as a capsid-E3-E2-6K-E1 polyprotein (or capsid-E3-E2-TF when frameshifting occurs). Capsid is autoproteolytically cleaved from the rest of the polyprotein (13). E3 serves as the signal sequence to translocate the rest of the

104 polyprotein into the endoplasmic reticulum (ER) (14, 15), where the cellular enzyme
105 signalase cleaves the polyprotein into E3-E2 (also known as pE2 or P62), 6K, and E1
106 (16, 17). When programmed ribosomal frameshifting occurs the protein pE2 and TF are
107 translated (5). In mammalian cells, the ER chaperones Erp57 and calnexin/calreticulin
108 regulate the folding and disulfide bond formation of E2 (18-20), and BiP and protein
109 disulfide isomerase do the same for E1 (18-22). pE2 and E1 form heterodimers within
110 the ER, before transiting to the Golgi where trimerization of the stable spike complex is
111 predicted to occur. Glycosylation of E2 and E1 occur in the ER and Golgi. In the ER and
112 Golgi, there is a slight decrease in pH and the E3 proteins acts as a clamp and prevents
113 low pH mediated dissociation of the E2-E1 heterodimer (23-25). These spikes in the
114 stable conformation are transported to the plasma membrane through the host
115 secretory system. In the late secretory pathway, the cellular enzyme furin cleaves E3
116 from E2, which acts as a priming event and converts the spike from the stable to
117 metastable conformation (26, 27). At the plasma membrane, E2 interacts with the
118 nucleocapsid core, and initiates budding and virus release. Particles may also bud from
119 glycoprotein-containing vesicles called cytopathic vesicles II, and this pathway is used
120 more by mosquito cells (28).
121 Voss et al. solved the Chikungunya virus (CHIKV) E2/E1 heterodimer in the
122 metastable conformation and in complex with E3 at neutral pH in the stable
123 conformation (29), and Li et al. solved the Sindbis virus (SINV) E2/E1 heterodimer at
124 acidic pH (30). These structures showed the intra-dimer contacts within a heterodimer.
125 Both groups fit the atomic heterodimers into cryo-EM structures of alphavirus virions to
126 identify inter-dimer interactions, or contacts between heterodimers within the spike, and

127 between the E2 and nucleocapsid core. E1 consists of three domains: I-III. Domain II
128 contains the fusion peptide and makes extended contacts with E2 in the intra-dimer
129 heterodimer (29-31). This intra-dimer interface contains the acid-sensitive region and
130 has been studied in regard to fusion regulation and mutations that expand vector range
131 (32, 33). E2 has three domains: A-C. Domain B is the most distal domain and acts as a
132 cap of the distal end of E1 protecting the fusion peptide (29, 30). In the low pH structure
133 by Li et al., Domain B was disordered suggesting it is the first portion of the heterodimer
134 to undergo conformational changes in response to low pH (30). Domain A in E2 is the
135 central domain and Domain C is the closest to the lipid bilayer. Domain C is sandwiched
136 between Domain II of E1 from its intra-dimer heterodimer and the Domain II of E1 from
137 the adjacent heterodimer, or E1'. Both Voss et al. and Li et al. identified residues in E2
138 Domain C that contact residues in Domain II of E1' (29, 30). Based on these two
139 structures, we hypothesized that E2 Domain C plays a key role in spike assembly, and
140 disrupting the inter-dimer contacts between E2 and E1' could affect trimer formation.
141 To test the role of Domain C in assembly, we substituted six amino acids in SINV E2
142 Domain C to the corresponding residues in CHIKV, an alphavirus in a different clade (2,
143 34). The E2 residues that were mutated are predicted to interact with E1' residues in the
144 adjacent dimer, or to "piggyback" on the dimers within a spike, and hence our mutant
145 was named Chikungunya Piggyback (CPB). We determined CPB had slower growth
146 and smaller plaques when grown in mammalian cells but not mosquito cells. CPB
147 quickly gained second-site revertants, E2-H333N and E1-S247L, which were each able
148 to restore growth in CPB. CPB grown in mammalian cells form particles with assembly
149 defects but the revertants restored their assembly to various degrees. Further analysis

150 of the spike conformations on the CPB by cryo-EM showed the spikes in CPB were
151 more flexible than the spikes in WT virus.
152
153 **RESULTS**
154 **Domain C of E2 is important for spike trimerization**
155 The atomic structure of the CHIKV E2/E1 heterodimer identified the interface
156 between E2 and E1 within a heterodimer and the intra-dimer contacts that were present.
157 When these heterodimers were placed into the cryo-EM density of intact SINV virions,
158 the potential contacts between heterodimers, or inter-dimer contacts, were identified
159 (Figure 1A-1C). In the virion, Domain C of the E2 protein was sandwiched between two
160 E1 proteins, one in the same heterodimer, designated as E1, and one from the adjacent
161 heterodimer, designated as E1' (Figure 1D, 1E) (29). We have colored the different
162 domains of E1 and E2 in Figure 1E to illustrate these interactions of Domain C of E2.
163 We hypothesized that Domain C would be important for spike trimerization because
164 these inter-dimer contacts would bridge or connect the individual E2-E1 dimers into
165 trimers.
166 Voss et al., identified ten residues in E2 Domain C that contact 12 residues in E1
167 Domain II in the adjacent heterodimer (29). In the low pH SINV E2/E1 heterodimer
168 structure, Li et al identified three residues in E2 Domain C that contact four residues in
169 E1′ Domain II, all also identified in the CHIKV structure (30). Residues E2-272 to E2-
170 288 in Domain C contained a majority of the E2 inter-dimer contacts (Figure 1F, 1G).
171 While there are 13 residues that differ between SINV and CHIK in the primary amino
172 acid sequence in the E2-272 to E2-288 region, only six of these residues are in contact

173 with E1' in the tertiary structure. Using SINV as our parental virus, we mutated the six
174 residues in this region from SINV to residues found in CHIKV, which belongs to a
175 different clade than SINV (Figure 1F, 1G) (2, 34). The resulting mutant was named
176 CHIK-Piggy-Back (CPB), as the SINV E1' residues "piggyback" on the six E2 residues
177 that were introduced from CHIKV. We opted to focus on the E2 inter-dimer residues
178 because there are fewer contact residues in E2 than E1 and we speculated that
179 mutating a larger number of residues in E1 would have increased the chance of
180 misfolding due to too many disrupted interactions within the E1 protein itself (21).
181

182 **Growth of CPB is attenuated in mammalian cells compared to in mosquito cells**

183 To determine the effect of our CPB mutation, we infected mammalian (BHK-21) and
184 mosquito (C6/36) cells at an MOI of 1 PFU/cell and quantified infectious virus release
185 over time. In BHK cells, the CPB growth was attenuated, producing virus 1 to 1.5 logs
186 lower titer than WT SINV (Figure 2A) as early as 8 hours post-infection. Additionally,
187 CPB had a mean plaque size of 1 mm compared to the mean plaque size of 2 mm for
188 WT SINV (Figure 3A, 3C). In C6/36 cells, however, CPB grew at a similar rate
189 compared to WT SINV (Figure 2B). BHK cells are typically grown at 37°C, while C6/36
190 cells are grown at 28°C. To rule out temperature dependence on growth, we also
191 measured WT SINV and CPB growth in BHK cells grown at 28°C. We found that there
192 was still a 1 to 1.5 log reduction in CPB titer relative to WT SINV (Figure 2C) suggesting
193 attenuated CPB growth is mainly an effect of different host cell environment, rather than
194 solely different temperatures.
195

196 **Two separate second-site revertants identified for CPB**

197 As we worked with the CPB virus, we noticed that the virus reverted quickly as
198 indicated by the change in plaque size phenotype from small to large. Changes in
199 plaque size were evident often after cells were infected more than 40 hours or
200 passaged more than two or three times (Figure 3A). To isolate revertants, we passaged
201 CPB in BHK cells and saw a mixed plaque phenotype. We isolated and plaque-purified
202 larger plaques, and then isolated and sequenced the viral RNA. We identified two
203 independent single-site revertants, E2-H333N and E1-S247L (Figure 3B). E2-H333N
204 was seen four times, and E1-S247L was seen once. Another mutation, E1-P250S, was
205 seen twice but only in combination with E2-H333N. We focused on E2-H333N and E1-
206 S247L since these single-sites potentially changed the virus fitness on their own. Both
207 the E2-H333N and E1-S247L mutations were in close proximity to the inter-dimer
208 interface (Figure 3B). E2-H333N is spatially near the six-residue cluster we mutated in
209 E2, approximately 13 Å away from the center of the E2 inter-dimer contacts. E1-S247L
210 is approximately 20 Å away from the center of the ten residues of E1' which interact with
211 the six residues of E2. SINV E1 is glycosylated at position 245. The E1-S247L mutation
212 abrogates the N-X-S/T motif needed for N-linked glycosylation at residue E1 245 (35),
213 by changing the Ser to Leu (Table 1).

214 To determine how these point mutations affect viral assembly, both of these
215 mutations were inserted back into CPB and the WT SINV virus. The plaque sizes of the
216 two revertants cloned into CPB were larger, comparable to that seen with WT SINV
217 virus. The mean plaque size of CPB E2-H333N was 1.6 mm and of CPB E1-S247L was
218 1.9 mm; both larger than CPB which was 1 mm (Figure 3C). Next, growth kinetics of

219 CPB E2-H333N and CPB E1-S247L were examined independently by infecting BHK
220 cells (Figure 3D). Both revertants resulted in a higher virus yield which grew between 1-
221 2 logs better than the parental CPB and at a similar rate as WT SINV, indicating that
222 both revertants rescued growth in CPB background. We also conducted growth kinetics
223 in C6/36 cells (Figure 3E) and observed no difference between the two revertants in
224 CPB, CPB and WT SINV. When the two mutations were independently cloned into the
225 WT SINV backbone and the viral growth examined in both BHK and C6/36 cells, we
226 observed no change in plaque size or growth kinetics. These results indicate that both
227 of the mutations are neither deleterious nor enhancing in the absence of the CPB
228 mutations.
229
230 **CPB particles show defects in spike incorporation compared to WT SINV**
231 Alphavirus spikes initially form dimers and then these dimers trimerize before
232 localizing to the plasma membrane. If the spikes do not trimerize, transport to the
233 plasma membrane is reduced. Spike trimerization is thought to be important for
234 alphavirus budding. In our CPB mutant, we used the alphavirus structures and targeted
235 residues that we thought would disrupt spike trimerization but not dimerization as
236 determined from Voss et al. and Li et al. (29, 30). To determine how particle budding
237 was affected in the CPB mutant, we looked at the composition and morphology of
238 purified virus particles from both BHK and C6/36 cells.
239 We purified virus particles through a sucrose cushion, ran them on an SDS-PAGE
240 gel, and examined the protein composition. We noticed that BHK purified CPB particles
241 have reduced amounts of E1 and E2 glycoproteins relative to capsid protein when

242 compared to the amounts of these proteins in WT SINV (Figure 4A). This could suggest
243 fewer spikes are associated with the virion and/or the associated spikes may easily
244 dissociate during the purification process compared with WT particles. The E1 protein
245 band in CPB E1-S247L migrates faster than E1 in WT SINV. The E1 protein in CPB E1-
246 S247L is at the same position as the E1 band in the SINV E1-N245/246Q virus which is
247 known to have one of the two E1 glycosylation sites disrupted resulting in a faster
248 migrating E1 protein band. As an additional control, the purified virion of SINV E1-
249 N139Q/E2-N318Q which has one E1 glycosylation site and one E2 glycosylation site
250 disrupted resulting in faster migration in both of those protein bands (Figure 4A) was
251 also included (35).
252 In contrast to BHK cells, C6/36 purified CPB particles showed similar amounts of E1
253 and E2 glycoproteins to WT SINV (Figure 4B), suggesting qualitatively that the amount
254 of spike proteins in released and purified particles were similar to WT SINV. The
255 revertants also had similar protein composition to WT SINV with CPB E1-S247L having
256 a faster migrating E1 protein band (Figure 4B). In both CPB and CPB E2-H333N virions,
257 the E2 protein is a smeared band suggesting heterogenous glycosylation on the E2
258 protein (36).
259
260 **CPB particles from mammalian cells show defects in particle morphology, which**
261 **are partially or fully rescued by revertants**
262 The reduced amount of glycoproteins in CPB particles suggested that the CPB
263 particle may be morphologically different compared to WT particles. To test this, we
264 stained our particles with uranyl acetate and imaged using transmission electron

265 microscopy (TEM). WT SINV is approximately 70 nm in size and spherical and this is
266 observed in both WT particles purified from BHK (Figure 4C) and C6/36 cells (Figure
267 4D). CPB, however, made almost no identifiable virus particles when purified from BHK
268 cells (Figure 4C). We also noticed that any visible particles were not spherical. CPB E2-
269 H333N partially rescued particle morphology while CPB E1-S247L fully recovered
270 particle morphology (Figure 4C). CPB E2-H333N made more particles than CPB, and
271 some of them looked to be around 70 nm in size; however, many non-spherical particles
272 were still seen. On the other hand, CPB E1-S247L made primarily spherical particles of
273 70 nm diameter, similar to WT SINV. In both CPB E2-H333N and CPB E1-S247L, there
274 are also small particles ranging in size of approximately 10-40 nm, which could be
275 assembly intermediates or disassembled fragments. These smaller particles suggest
276 that CPB E2-H333N and CPB E1-S247L particles may still be fragile compared to WT
277 SINV, despite being just as infectious.
278 WT SINV, CPB, and revertant virus particles purified from C6/36 were spherical and
279 homogenous in shape, consistent with no major assembly or growth defects (Figure
280 4D). CPB particles appeared to have dimples or creases. This could suggest that even
281 in C6/36 cells the mutations made in CPB are detrimental to proper spike formation or
282 have defects in assembly but are still good enough that infectious particle assembly
283 occurs (28).
284
285 **Glycoprotein transport is not significantly affected in CPB**
286 The low amounts of glycoproteins in CPB virions compared to WT SINV virions from
287 BHK cells led us to two hypotheses. One, CPB has defects in spike trimerization and

288 transport to the plasma membrane is diminished. Or second, CPB virions are
289 misassembled because inter-dimer contacts have been disrupted. As a result, CPB may
290 disassemble more than WT SINV during the purification process. These options are not
291 mutually exclusive.

292 We used immunofluorescence to test if glycoprotein transport was altered in CPB
293 compared to WT SINV. We infected BHK cells at an MOI of 2 PFU/cell for ten hours, a
294 time where there was a difference in infectious particles released and probed for
295 glycoproteins at the cell membrane (Figure 5). Cells were fixed with paraformaldehyde,
296 a non-permeabilizing fixative, and probed for SINV glycoproteins. Under these infection
297 conditions, cells were not displaying CPE (Figure 5A, 5C). There was no drastic
298 difference in glycoprotein levels at the plasma membrane between WT SINV, CPB, and
299 revertant infected cells (Figure 5C, 5D). Virus-infected cells were equally healthy and
300 had comparable amounts of detectable glycoproteins.

301

302 **Spikes in CPB particles are distorted compared to WT SINV**

303 The difference in particle morphology between CPB and WT SINV in mammalian
304 cells was striking when imaged by TEM (Figure 4C, 4D). To further examine the particle
305 structure and spike morphology, we purified virions and used cryo-EM to solve their 3D
306 reconstructions. We focused on WT SINV, CPB, and the revertant CPB E1-S247L since
307 these had the most extreme phenotypes and their structures would be most clear by
308 cryo-EM (Figure 6). We imposed icosahedral averaging (Table 2) during the
309 reconstruction process. The overall structural organizations of all six particles (WT
310 SINV, CPB, CPB E1-S247L from BHK and C6/36) were preserved (Figure 6A-F). There

311 are 80 petal-like spikes arranged into a T=4 surface lattice; the white triangle delineates
312 one asymmetric unit (Figure 6A) (37). No clear E3 density was observed in any of the
313 particles, consistent with what has been previously observed with SINV (8). The glycan
314 modification at E2-196, located at the distal end of the E2 protein, was clearly seen
315 when the estimated resolution is better than 10 Å (red arrows). As seen in other
316 alphavirus structures (7, 38-42), the E1 protein contributes to the continuous shell
317 underneath the spikes (Figure 6A-F, yellow color) with holes at every twofold and
318 fivefold above the membrane. Note the resolution of the particles range from 4.5 Å to
319 10.7 Å, which reflects both the number of particles used in the reconstruction (Table 2)
320 and the heterogeneity of the particles themselves.
321 However, when looking more carefully at the enlarged view of each spike at the
322 quasi-threefold axis, (dotted circle Figure 6A), there were discernable differences
323 between the samples (Figure 6G-L). We chose the quasi three-fold spike because
324 spikes at the 5-, 3-, 2- fold would, by default of icosahedral symmetry, be identical. The
325 spikes at the quasi symmetry axes would not have any symmetry imposed on them and
326 differences in morphology would be more evident. To best compare the quasi-three
327 spikes, we show them all at 10.7 Å, the resolution of CPB from BHK cells. The irregular
328 density at the inter-dimer location of the spike was clearest in CPB purified from BHK
329 cells (Figure 6H, black arrows). Note that the density of two lobes at the spike petal
330 were fused together, while the other heterodimer within the same spike remained
331 separate (Figure 6H, BHK CPB). For the other five particles, the E1/E2 dimers within a
332 spike were organized in a trimeric manner with true trimeric symmetry.
333

334 **DISCUSSION**

335 To investigate the role of the inter-dimeric contacts in assembly, we used a
336 structure-guided approach and mutated six residues in E2 that, in the stable and
337 metastable structures of the spike, are at the interface with the adjacent E1' protein
338 (Figure 1) (29, 30). We called this mutant CPB. We found that CPB growth is attenuated
339 in mammalian cells compared to mosquito cells (Figure 2). In mammalian cells, CPB
340 glycoprotein expression on the cell surface is similar to WT SINV (Figure 5), but the
341 released particles show CPB particle composition and morphology is defective in
342 mammalian cells while minimally affected in mosquito cells (Figure 4). Our cryo-EM
343 structures of CPB show that CPB particle spikes do not have three symmetrical lobes.
344 Figure 6 shows a visible gap between two of the lobes and the third, which could
345 suggest that two heterodimers are interacting but the third is not. The mutations in E2
346 disrupt inter-dimer contacts and we hypothesized that CPB growth falls behind WT
347 SINV because of its subsequent assembly defects. However, it is difficult to separate
348 assembly defects from downstream entry impacts.

349 The difference in phenotype in mammalian and mosquito cells suggests that there is
350 a host factor that is involved in the trimerization of E2-E1 heterodimers since the same
351 viral proteins are assembling in each host cell. If this assembly was autonomous, we
352 would not observe a host-specific difference in both infectious particle production and
353 particle morphology. These differences could be due to different post-translational
354 modifications by the host, different host-protein chaperones affecting virus assembly, or
355 a combination of both. BHK and C6/36 cells are defective some innate immune
356 responses so the attenuation in growth is not entirely a host response to infection. The

357 CPB mutant and its revertants will be useful to identify host chaperones important in
358 spike assembly.
359
360 **Stability, composition, and conformation of CPB and revertant spikes**
361 Our immunofluorescence results show that glycoprotein transport to the plasma
362 membrane is comparable between CPB and WT SINV. However, nothing about the
363 conformation of the spikes can be concluded. Furthermore, while E2-E1 are most stable
364 as heterodimers, small amounts of the monomeric proteins will localize to the plasma
365 membrane (15). Our results cannot differentiate conformation or oligomeric state of the
366 glycoproteins at the cell surface.
367 It is perplexing that we can obtain a structure of CPB purified from BHK cells when
368 this same sample shows few particles by negative-stain TEM and there were low levels
369 of glycoproteins when we look at particle composition on an SDS-PAGE gel (Figure 4).
370 There are several possibilities for these discrepancies, and likely more than one is a
371 contributing factor.
372 Due to the trimerization defect, fewer spikes may be incorporated into virus particles,
373 and those that are on the particle may be more heterogenous compared to WT SINV.
374 The CPB trimer has a different conformation than the WT SINV trimer, it could also be
375 that the cytoplasmic domain of E2 is no longer able to interact with capsid in a 1:1 ratio
376 and this affects titer and particle stability. The reduced number of spikes on the particles
377 explains the lower titers (Figure 2) and why purified particles show lower amounts of
378 spike proteins in CPB compared to WT SINV (Figure 4). Our cryo EM results also
379 support this hypothesis. We used roughly 16,000 CPB and CPB E1-S247L particles

380 each from BHK infected cells for our reconstructions. Yet the resolutions of the final
381 structures were ~11Å and 6Å respectively, suggesting more heterogenous particles for
382 CPB than the revertant. WT SINV only used 9,000 particles and a resolution of 8Å was
383 obtained. From our cryo-EM reconstructions, we can see heterogeneity in the individual
384 spikes of CPB compared to WT SINV and CPB E1-S247L particles. Interestingly, our
385 TEM images show that CPB S247L produces particles that are much more WT-like than
386 CPB H333N, despite both revertants restoring CPB growth.
387 Together the lower number of spikes and their misassembly and heterogeneity could
388 account for particle instability. Fewer spikes on the surface means there is no E1 lattice
389 that covers the viral envelope. The particles are more fragile and sensitive to chemicals.
390 Particles are dehydrated and treated with an acidic stain when preparing for negative
391 stain imaging, and as a result, particles may disassemble or aggregate. In contrast,
392 flash freezing the samples for cryo preservation has a mild effect on the particle's
393 integrity so misassembled particles will be frozen and can be analyzed.
394
395 **Possible implications of revertant residues**
396 CPB quickly reverted resulting in two independently fit mutations, E2-H333N and E1-
397 S247L, and one mutation, P250S, which was seen only in combination with E2 H333N.
398 E2-H333N, E1-S247L, and P250S are all in close proximity to the cluster of mutations
399 made at the inter-dimer interface, although none were identified by Voss or Li as one of
400 the inter- or intra-dimer contact residues (29, 30). Residue 333 for most viruses is either
401 a histidine or an asparagine. Additionally, the corresponding residue for SINV H333 is
402 N330 in CHIKV. Because the histidine side chain has a pKa of 6.00, it is within the

403 range of different pH environments in the host cell. This histidine residue may affect
404 CPB either during entry, specifically during disassembly in the endosome (43, 44), or
405 during assembly as the E2-E1 heterodimer travels through the ER and Golgi (45). The
406 role in disassembly could be unfavorable in CPB, since it may have a less stable trimer
407 and less stable heterodimers even without a low pH environment. During assembly of
408 the CPB E2-E1 heterodimers, there may be improper folding possibly making trimer
409 assembly more sensitive to pH which cannot occur with H333.

410 S247L interferes with N-linked glycosylation motif that allows E1-N245 to be
411 glycosylated. In CHIKV, there is only one glycosylation site on E1 at N141 versus two in
412 SINV, one at N139 and one at N245 (Table 1) (35, 38). Although residue 247 is not
413 conserved among alphaviruses, it is clear that some viruses including SINV have the N-
414 X-S/T glycosylation motif at N245, while others including CHIKV do not. It is interesting
415 that CPB S247L appears more WT-like in particle morphology than CPB H333N. It is
416 possible that de-glycosylation at this site allows for better folding or removes a steric
417 hinderance that allows for trimerization.

418 From our revertant sequencing we also saw that in some instances when E2-H333N
419 was mutated, E1-P250S was also mutated. Residue 250 is a proline residue in SINV
420 and a serine residue in CHIKV. It was seen with H333N but does not seem necessary
421 for restoring growth since H333N was seen alone two times and CPB H333N
422 independently restored growth. However, the proline residue in CPB might disrupt
423 folding since it is unable to form hydrogen bonds. This could explain why CPB H333N
424 has less spherical looking particles, despite having growth comparable to that of WT
425 SINV. In all three cases, it appears that CPB is reverting to be more like CHIKV.

426

427 **Other revertants in spike proteins that show host specificity**

428 Our work is not the first time a mutation has shown host specificity in alphaviruses.
429 In CHIKV, Ashbrook et al., showed a mutation at E2 G82R enhanced infectivity in
430 mammalian cells but reduced infectivity in mosquito cells and reduced virulence in
431 mouse model (46). This residue is present on the exterior of the E2 protein and was
432 determined to be important to GAG binding, entry and virulence.

433 Jupille et al. identified Ross River E2 Y18H as having a fitness advantage in
434 mosquito cells and a disadvantage in mammalian cells (47). This residue lies in the
435 intra-dimer interface of the E2-E1 heterodimer. Interestingly, in the Ross River clade,
436 the viruses have either a tyrosine or a histidine at position 18 and the authors suggest,
437 this residue serves as a regulator of fitness between the mosquito vector and
438 mammalian host (47). In our work, the revertant E2 H333N was isolated. Most
439 alphaviruses are either a histidine or asparagine at this residue emphasizing the
440 structural and functional requirement of this residue.

441 Our work presented here is the first example of a mutation that has host specificity
442 and mapping to defects in spike assembly. Further work needs to be done to dissect the
443 exact mechanism of where in the spike assembly pathway the CPB mutant fails in
444 mammalian cells and how the revertants overcome these defects. Presented results
445 now allow us to further identify host-specific chaperones and factors necessary for
446 alphavirus glycoprotein folding and oligomerization and possibly extend to other
447 arboviruses that assemble in multiple host environments.

448

449 **Materials and Methods**

450 **Viruses and cells**

451 The virus strains used in this work were the TE12 strain of SINV and 181/21 strain of
452 CHIKV (a gift from Dr. Terrence Dermody). BHK-21 cells (BHK) (American Type Culture
453 Collection, Manassas, VA) were grown in minimal essential medium (Mediatech,
454 Manassas, VA) supplemented with 10% fetal bovine serum (FBS; Atlanta Biologicals,
455 Lawrenceville, GA), nonessential amino acids, L-glutamine, and antibiotic-antimycotic
456 solution (Corning, Corning, NY). BHK-21 cells were grown at 37°C in the presence of
457 5% CO_2, or at 28°C in the presence of 5% CO_2. C6/36 cells (American Type Culture
458 Collection, Manassas, VA) were grown in identical medium at 28°C in the presence of
459 5% CO_2.

460

461 **Generation of wild-type and mutant viruses**

462 The CPB mutant virus was generated using a two part QuikChange site-directed
463 mutagenesis (Agilent, Santa Clara, CA) of the TE12 SINV cDNA clone. First the
464 residues between nucleotides 9444 and 9494 were deleted, and then the chimera
465 sequence was inserted. No additional changes were introduced to the chimera virus
466 during cloning. The mutations were confirmed by sequencing the E2 region. The CPB
467 E2-H333N and CPB E1-S247L were generated by QuikChange site-directed
468 mutagenesis.

469 Wild-type and mutant cDNA clones were linearized with Sac I and in vitro
470 transcribed with SP6 polymerase at 39°C for 2 hr. For electroporation of BHK cells,
471 approximately 10^7 BHK cells were trypsinized, washed two times with phosphate-

472 buffered saline (PBS), and resuspended with PBS to a final volume of 500 µl. The cells
473 were mixed with *in vitro*-transcribed RNA in a 2-mm-gap cuvette and pulsed once at 1.5
474 kV, 25 µF, and 200 Ω using a Bio-Rad Gene Pulser Xcell electroporation system (Bio-
475 Rad Laboratories, Hercules, CA). Following a 5-min recovery at room temperature, the
476 cells were diluted 1:10 in cell medium and incubated at 37°C in the presence of 5%
477 CO_2. At the indicated time points (around 24 hours post infection for WT, CPB E2-
478 H333N, CPB E1-S247L, and 40 hours post infection for CPB), virus was harvested, and
479 the titer was determined using a standard plaque assay procedure (23). Plaques were
480 detected at 48 hours post-infection by formaldehyde fixation and crystal violet staining.
481

482 **One-step growth analysis**

483 Confluent 12-well plates of BHK cells were infected with virus at MOI of 1 PFU/cell at
484 room temperature for 1 hr. Following this adsorption period, the cells were washed with
485 PBS to remove any unbound particles, and 400 µL of media was added. At the
486 indicated time points, 400 µL media was removed and replaced with fresh media. The
487 titers of these samples were determined by standard plaque assay and plotted against
488 time. *P* values were calculated using Welch's unpaired *t* test.
489

490 **Identification of second-site revertants**

491 Large plaques were detected from media of CPB infected BHK cells more than 40
492 hours post-electroporation. As previously described (23), large plaques were isolated
493 and used to infect BHK cells. The infected cells were lysed at 14 hours post-infection
494 with TRIzol reagent (Invitrogen, Carlsbad, CA), and cytoplasmic RNA was isolated

495 using chloroform extraction. The coding sequence of the structural polyprotein was
496 amplified from the viral RNA using RT-PCR and two primers, one specific for the E1
497 region and the other specific for the E2 region. The region corresponding to the
498 structural polyprotein was sequenced to identify the location of the potential second-site
499 mutation. To verify that the large plaque phenotypes were due to the mutation identified
500 in sequencing, the revertant sites were introduced back into the chimeric viruses and
501 growth kinetics and plaque sizes were analyzed.
502

503 **Virus purification**

504 150 mm dishes were infected with 3 mL virus at a MOI of 0.1 PFU/cell at room
505 temperature for 1 hr. After the adsorption period, the cells were overlaid with 15 mL
506 serum-free media (Thermo Fisher Scientific life technologies, Waltham, MA)
507 supplemented with nonessential amino acids, L-glutamine, and antibiotic-antimycotic
508 solution (Corning). Medium was collected approximately 24 hours post infection for BHK
509 cells. For C6/36 cells, 5 mL fresh serum-free media was added after 72 hours, and
510 medium was collected after approximately 120 hours post infection. The medium was
511 then spun down at 1157 × g for 5 min at 15°C to remove cells and cell debris. Virus
512 particles from the clarified medium was pelleted through sucrose cushion. The clarified
513 medium was overlaid onto 3 ml 27% sucrose in 20 mM HN buffer (20 mM HEPES, pH
514 7.5, and 150 mM NaCl) and spun at 140,000 × g for 2.5 h at 15°C (36, 48).
515

516 **SDS PAGE gel of purified virus particles**

517 Purified virus particles were loaded onto an 8% SDS gel containing 0.5% 2,2,2-
518 trichloroethylene v/v in the resolving gel, and run for approximately 45 minutes at 200 V.
519 The gel was imaged with the Bio-Rad ChemiDoc MP Imaging System using the stain-
520 free image setting. The PageRuler prestained protein ladder (Thermo Fisher Scientific-
521 Invitrogen, Waltham, MA) was used in all studies.
522

523 **Immunofluorescence analysis of cell surface spike protein expression**

524 SINV was purified from BHK and C6/36 cells. The purified particles were ran on an
525 SDS-PAGE gel and the glycoprotein bands were excised and sent to Cocalico
526 Biologics, Inc (Stevens, PA) to generate polyclonal antibodies. The primary antibodies
527 were pre-cleared to reduce background signal from non-specific cell binding. A
528 confluent well of BHK cells was washed twice with PBS, chilled with PBS for 2 hours,
529 and then incubated at 4°C with 200 µL of a 1:10 dilution of antibody in cold PBS for 2
530 hours while rocking. The antibody mixture was removed and centrifuged, and the
531 supernatant was saved and used in immunofluorescence studies.

532 BHK cells were grown on coverslips and at approximately 75% confluency were
533 infected with virus at an MOI of 2 PFU/cell at room temperature for 90 minutes. After
534 this adsorption period, fresh media was added, and cells were incubated at 37°C in the
535 presence of 5% CO_2. Ten hours post infection, the cells were washed with PBS and
536 then fixed with 4% paraformaldehyde (Thermo Fisher Scientific Life Technologies,
537 Waltham, MA) at room temperature for 10 minutes. 16% EM-grade paraformaldehyde
538 was diluted in PBS to make 4% paraformaldehyde; the EM-grade paraformaldehyde is
539 methanol-free to avoid permeabilization. The cells were then washed, blocked in 2.5%

540 BSA in PBS for 30 minutes, and incubated with pre-cleared polyclonal anti-E2/E1 (1:50
541 of pre-cleared) in 2.5% BSA for 45 minutes. Cells were washed and incubated with
542 Alexa 488 Goat anti-Rabbit secondary antibody (1:5000) in 2.5% BSA in PBS for 45
543 minutes in the dark. Cells were then washed and stained with DAPI. The coverslips
544 were carefully removed, dipped in distilled water and blotted, and inverted onto 5 μL of
545 Aqua-Poly/Mount (Polysciences, Warrington, PA) on a slide. Slides were imaged using
546 an Olympus 1X71 fluorescence microscope (Olympus, Center Valley, PA).
547

548 **Transmission electron microscopy**

549 Four μL of purified virus was applied to a Formvar- and carbon-coated 400-mesh
550 copper grid (Electron Microscopy Sciences, Hatfield, PA) for 25 seconds, washed with 4
551 μL water for 25 seconds, and stained with 2% uranyl acetate for 25 seconds. The
552 stained grids were analyzed using a JEOL 1010 transmission electron microscope
553 (Tokyo, Japan) operating at 80 kV. Images were recorded using a Gatan UltraScan
554 4000 charge-coupled-device camera (Pleasanton, CA).
555

556 **Cryo-EM imaging and 3D reconstruction**

557 To prepare a frozen-hydrated cryo-EM specimen, approximately 4 μL of purified
558 virus sample was applied to a glow-discharged 300-mesh copper grid coated with
559 continuous carbon film (Electron Microscopy Sciences, Hatfield, PA). The grid was
560 plunged into a liquid ethane container that is further cooled by a liquid nitrogen bath.
561 This process was performed using Vitrobot Mark IV under 4 degree and 100% humidity
562 (Thermo Fisher Scientific-Invitrogen, Waltham, MA). Frozen-hydrated cryo-EM grids for

563 all samples except SINV WT (C6/36) were clipped into cartridges and then transferred
564 into a cassette according to the manufacture protocol. The cassette was loading inside
565 a 300-kV Titan Krios G3i equipped with Gatan BioContinuum™ K3 direct electron
566 detection camera. Data acquisition was set up using TFS EPU under counted super-
567 resolution mode. The nominal magnification is 64,000x (equal to 0.7 Å per pixel) and the
568 illumination has a dose rate of 1 $e^-/Å^2$ per frame under the exposure preset with a total
569 dose of 30 $e^-/Å^2$. Zero-loss peak was aligned every hour with an energy slit opened at
570 20 eV. Data collection for SINV WT (C6/36) was done by using a 300-kV JEOL JEM-
571 3200FS TEM equipped with DE-12 CMOS camera (Direct Electron). The frozen
572 hydrated grid was transferred to a Gatan 626 cryo-holder and inserted into the TEM.
573 The nominal magnification was set to 80,000x (equal to 1.9 $e^-/Å^2$). The zero-loss peak
574 was aligned at the beginning of the data collection with a slit opened at 20 eV. The total
575 accumulated dose is ~30 $e^-/Å^2$.
576 Image analysis was performed using Relion (v3.1) (49). Initial particle picking was
577 done by Laplacian-of-Gaussian filtered auto-picking method implemented in Relion (50).
578 Subsequently, 2D classification was used to eliminate the noise density that got picked
579 earlier and the 3D initial model was built de novo. This initial model was then used as a
580 template for automatic particle picking for all samples. Similarly, multiple runs of 2D
581 classification and 3D refinement were performed to obtain the final 3D models
582 (summarized in Table 2). Each volume was rendered using UCSF ChimeraX (51).
583

584 **Acknowledgements**

585 We thank IU Virology group for constructive discussions and Jim Powers, Walczak
586 and Shaw labs and the IU Light Microscopy Facility. Funding for this work from IU Wells
587 Scholars Program and LS McClung Fellowship (SCR), the startup fund from The
588 Pennsylvania State University College of Medicine to J.C.-Y.W and IU IAS (SM). We
589 also gratefully acknowledge The Pennsylvania State University College of Medicine for
590 access to the Cryo-EM (RRID:SCR_021178) and the HPC core facilities.

591

592 **FIGURE LEGENDS**

593 **Figure 1: Inter-dimer interface residues in Domain C of E2 may be important for**
594 **spike assembly.** (A) Crystal structure of CHIKV glycoproteins E2 (blue) and E1 (yellow)
595 (PDB ID: 3N40) (29) fit into cryo-EM map of SINV (PDB ID:1Z8Y) (29). One trimeric
596 spike is outlined. (B) During assembly, E1 (*shades of yellow*) forms heterodimers with
597 E2 (*shades of blue*), and these dimers then trimerize. A top view of one of these trimeric
598 spikes, with the individual E2 (in teal, light blue, and blue) and E1 (in gold, light yellow,
599 and saffron) proteins is shown here. A total of 80 spikes are on the surface of the
600 alphavirus particle. (C) The trimer is rotated 90 degrees for a side view. The light blue
601 E2 and light yellow E1 are a heterodimer. Intra-dimer contacts occur between Domains I
602 and II of E1 with Domains A, B, C of E2. The teal E2' and gold E1' form another
603 heterodimer, with similar intra-dimer contacts. The last dimer in the spike is shown in
604 grey. (D) A 60-degree rotation of (C) highlights an inter-dimer interface in the trimer.
605 Inter-dimer contacts are between the gold E1' of one heterodimer and the light blue E2
606 in the adjacent dimer. Domain C of E2 (red dashed circle) is sandwiched between the
607 adjacent E1' (gold) and its cognate E1 (light yellow), forming inter-dimer and intra-dimer

608 contacts, respectively. (E) The same proteins, E1', E2, and E1, shown in (D) are color
609 coded by domain here. Domain III of E1/E1' is dark green, Domain I of E1/E1' is yellow-
610 green, and Domain II of E1/E1' is yellow. Domain C of E2 is in dark purple and Domain I
611 and II are in light purple. The other monomers are colored gray for clarity. (F) Ribbon
612 diagram of the inter-dimer of E1'-E2. Residues in E1' that contact E2 are in yellow
613 residues in E2 that contact E1' are in blue spheres (light and dark). The residues
614 mutated in this study are in dark blue spheres. (G) Amino acid alignment of CHIKV and
615 SINV E2 in the inter-dimer region; SINV residues shown in black and CHIKV residues
616 shown in red. The CHIK-Piggy-Back (CPB) chimera was generated by substituting the
617 non-homologous E2 CHIKV residues for the corresponding SINV E2 residues
618 (*highlighted in red in CPB)* in this region.
619
620 **Figure 2: CPB grows slower than WT SINV in mammalian cells compared to in**
621 **mosquito cells.** Cells were infected at an MOI of 1 PFU/cell. At the indicated time
622 points, media was collected and replaced with fresh media. The titers of the collected
623 samples were determined by standard plaque assay on BHK cells. Results are shown
624 for one representative experiment (N=5). (A) Growth kinetics of infectious virus released
625 from BHK cells at 37°C show CPB was attenuated by 1-1.5 logs relative to WT SINV.
626 (B) Growth kinetics of virus grown in C6/36 cells at 28°C show CPB releases infectious
627 particles at the same rate as WT SINV. (C) Growth kinetics of virus grown in BHK cells
628 at 28°C show that CPB growth is still attenuated by 1-1.5 logs relative to WT SINV.
629

630 **Figure 3: Two CPB revertants map close to the inter-dimer interface and grow**
631 **similarly to WT SINV.**

632 (A) CPB collected 20-40 hours post-electroporation have smaller plaques compared to
633 WT SINV plaques ($p<0.0015$, see 3C). When CPB is harvested later, or as it is
634 passaged in BHK cells, larger plaques are seen in addition to the small plaques. Five of
635 these larger plaques were isolated, the RNA was sequenced, and two independent
636 second-site revertants were found. (B) The locations of two second-site revertant sites,
637 H333N in E2 (*cyan*) and S247L in E1 (*red)*, are shown in the E1'-E2 dimer. E1' and E2
638 contact residues are colored in yellow and blue, respectively, as they were in Figure 1F;
639 mutated sites in CPB are in dark blue. (C) CPB E2-H333N and CPB E1-S247L were
640 introduced independently into CPB. Plaque size of CPB E2-H333N and CPB E1-S247L
641 in BHK cells was larger compared to CPB and not significantly (ns) different from WT.
642 (D) Growth kinetics of the two revertants show they have comparable titers as WT SINV
643 in BHK and (E) C6/36 cells. Representative curves are shown (N=3). Cells were
644 infected at an MOI of 1 PFU/cell, media was collected at the indicated time points, and
645 samples titered on BHK cells.

646

647

648 **Figure 4: Particle morphology and composition is restored in CPB revertants to**
649 **varying degrees.** Cells were infected at a MOI of 0.1 PFU/cell for 1 hour, after which
650 serum-free media was overlayed. Infected BHK media was collected after 24 hours, and
651 infected C6/36 media was collected after 120 hours. The media was clarified and
652 purified through a sucrose cushion at 140,000 × g for 2.5 h. (A and B) To determine the

653 composition of the virions, purified virus was solubilized in reducing SDS sample buffer,
654 run on an 8% SDS-PAGE gel, and imaged by stain-free TCE. CPB particles have a
655 reduced level of E2/E1 glycoproteins in particles purified from BHK cells. The E1
656 deglycosylation control is SINV E1-N245/246Q, which has one of its two E1
657 glycosylation sites deglycosylated resulting in a faster migrating E1 protein band, and
658 the E1/E2 deglycosylation control is E1-N139Q/E2-N318Q and has a deglycosylation
659 site in both E1 and E2 resulting in faster migration in each of those protein bands. (C
660 and D) Purified particles were applied to a Formvar- and carbon-coated 400-mesh
661 copper grid, stained with 2% uranyl acetate, and imaged at ×20,000 magnification with
662 the JEOL 1010 transmission electron microscope. Scale bar for TEM = 200nm.
663
664 **Figure 5: CPB glycoprotein spikes are transported to the plasma membrane of**
665 **BHK cells in approximately equal amounts compared to WT.** BHK cells were
666 infected at an MOI of 2 PFU/cell. Ten hours post-infection, the cells were fixed with 4%
667 EM-grade paraformaldehyde and probed for SINV E1/E2. Images were taken at ×40
668 magnification on a Nikon Ni-E microscope. Representative images are shown (N=4). (A)
669 Brightfield images and (B) DAPI staining show cells in field of view and their nuclei in
670 blue. (C) Cell surface E2/E1 expression shown in green, Alexa Fluor 488 was the
671 secondary antibody. (D) Anti-E2/E1+DAPI merge shows green fluorescence from
672 surface glycoprotein expression relative to the cells present.
673
674 **Figure 6. Cryo-EM 3D reconstructions show that CPB spikes from mammalians**
675 **cells have an altered interdimer organization.** (A-F) Radially colored isosurface

676 rendering of WT SINV, CPB, and SINV E1-S247L from BHK cells (A-C, top row) and
677 C6/36 cells (D-F, bottom row). All views are at the 5-fold axis. All six maps have a
678 similar outer appearance with 80 spikes decorating a fenestrated surface. In (A), the
679 white triangle shows one asymmetric unit. Filled oval, triangle, and pentagon indicate
680 locations of twofold, threefold and fivefold axes, respectively. The dotted circle shows
681 one of the spikes on the quasi-three axis. (G-L) Enlarged views of SINV spikes at the
682 quasi-threefold location, all images shown at 10 Å resolution for comparison purposes.
683 The spike of CPB from BHK (H) shows a distinct organization from other SINV spikes.
684 Black arrowheads indicate the difference in the electron density between each
685 interdimer interface. Red arrowheads show glycan modification at E2-196.

686

687 **REFERENCES**

688

689 1. Griffin DE. 2013. Chapter 23: Alphaviruses, p 652-770. *In* Knipe DM, Howley PM
690 (ed), Fields' Virology. Lippincott Williams & Wilkins, Philadelphia, PA.

691 2. Kuhn RJ. 2013. Chapter 22: Togaviradae, p 629-650. *In* Knipe DM, Howley PM
692 (ed), Fields' Virology. Lippincott Williams & Wilkins, Philadelphia.

693 3. Hermanns K, Marklewitz M, Zirkel F, Overheul GJ, Page RA, Loaiza JR, Drosten
694 C, van Rij RP, Junglen S. 2020. Agua Salud alphavirus defines a novel lineage of
695 insect-specific alphaviruses discovered in the New World. J Gen Virol 101:96-
696 104.

697 4. Forrester NL, Palacios G, Tesh RB, Savji N, Guzman H, Sherman M, Weaver
698 SC, Lipkin WI. 2012. Genome-scale phylogeny of the alphavirus genus suggests
699 a marine origin. J Virol 86:2729-38.

700 5. Firth AE, Chung BY, Fleeton MN, Atkins JF. 2008. Discovery of frameshifting in
701 Alphavirus 6K resolves a 20-year enigma. Virol J 5:108.

702 6. Chen R, Mukhopadhyay S, Merits A, Bolling B, Nasar F, Coffey LL, Powers A,
703 Weaver SC, Ictv Report C. 2018. ICTV Virus Taxonomy Profile: Togaviridae. J
704 Gen Virol 99:761-762.

705 7. Cheng RH, Kuhn RJ, Olson NH, Rossmann MG, Choi HK, Smith TJ, Baker TS.
706 1995. Nucleocapsid and glycoprotein organization in an enveloped virus. Cell
707 80:621-30.

708 8. Tang J, Jose J, Chipman P, Zhang W, Kuhn RJ, Baker TS. 2011. Molecular links
709 between the E2 envelope glycoprotein and nucleocapsid core in Sindbis virus. J
710 Mol Biol 414:442-59.

711 9. Jose J, Przybyla L, Edwards TJ, Perera R, Burgner JW, 2nd, Kuhn RJ. 2012.
712 Interactions of the cytoplasmic domain of Sindbis virus E2 with nucleocapsid
713 cores promote alphavirus budding. J Virol 86:2585-99.

714 10. Lee S, Owen KE, Choi HK, Lee H, Lu G, Wengler G, Brown DT, Rossmann MG,
715 Kuhn RJ. 1996. Identification of a protein binding site on the surface of the
716 alphavirus nucleocapsid and its implication in virus assembly. Structure 4:531-41.

717 11. Skoging U, Vihinen M, Nilsson L, Liljestrom P. 1996. Aromatic interactions define
718 the binding of the alphavirus spike to its nucleocapsid. Structure 4:519-29.

719 12. Zhao H, Lindqvist B, Garoff H, von Bonsdorff CH, Liljestrom P. 1994. A tyrosine-
720 based motif in the cytoplasmic domain of the alphavirus envelope protein is
721 essential for budding. EMBO J 13:4204-11.

722 13. Melancon P, Garoff H. 1987. Processing of the Semliki Forest virus structural
723 polyprotein: role of the capsid protease. J Virol 61:1301-9.

724 14. Mayne JT, Rice CM, Strauss EG, Hunkapiller MW, Strauss JH. 1984.
725 Biochemical studies of the maturation of the small Sindbis virus glycoprotein E3.
726 Virology 134:338-57.

727 15. Lobigs M, Zhao HX, Garoff H. 1990. Function of Semliki Forest virus E3 peptide
728 in virus assembly: replacement of E3 with an artificial signal peptide abolishes
729 spike heterodimerization and surface expression of E1. J Virol 64:4346-55.

730 16. Liu N, Brown DT. 1993. Transient translocation of the cytoplasmic (endo) domain
731 of a type I membrane glycoprotein into cellular membranes. J Cell Biol 120:877-
732 83.

733 17. Harrington HR, Zimmer MH, Chamness LM, Nash V, Penn WD, Miller TF, 3rd,
734 Mukhopadhyay S, Schlebach JP. 2020. Cotranslational folding stimulates
735 programmed ribosomal frameshifting in the alphavirus structural polyprotein. J
736 Biol Chem 295:6798-6808.

737 18. Mulvey M, Brown DT. 1996. Assembly of the Sindbis virus spike protein complex.
738 Virology 219:125-32.

739 19. Molinari M, Helenius A. 1999. Glycoproteins form mixed disulphides with
740 oxidoreductases during folding in living cells. Nature 402:90-3.

741 20. Molinari M, Helenius A. 2000. Chaperone selection during glycoprotein
742 translocation into the endoplasmic reticulum. Science 288:331-3.

743 21. Mulvey M, Brown DT. 1994. Formation and rearrangement of disulfide bonds
744 during maturation of the Sindbis virus E1 glycoprotein. J Virol 68:805-12.

745 22. Mulvey M, Brown DT. 1995. Involvement of the molecular chaperone BiP in
746 maturation of Sindbis virus envelope glycoproteins. J Virol 69:1621-7.

747 23. Snyder AJ, Mukhopadhyay S. 2012. The alphavirus E3 glycoprotein functions in
748 a clade-specific manner. J Virol 86:13609-20.

749 24. Uchime O, Fields W, Kielian M. 2013. The role of E3 in pH protection during
750 alphavirus assembly and exit. J Virol 87:10255-62.

751 25. Sjoberg M, Lindqvist B, Garoff H. 2011. Activation of the alphavirus spike protein
752 is suppressed by bound E3. J Virol 85:5644-50.

753 26. Lobigs M, Garoff H. 1990. Fusion function of the Semliki Forest virus spike is
754 activated by proteolytic cleavage of the envelope glycoprotein precursor p62. J
755 Virol 64:1233-40.

756 27. Zhang X, Fugere M, Day R, Kielian M. 2003. Furin processing and proteolytic
757 activation of Semliki Forest virus. J Virol 77:2981-9.

758 28. Jose J, Taylor AB, Kuhn RJ. 2017. Spatial and Temporal Analysis of Alphavirus
759 Replication and Assembly in Mammalian and Mosquito Cells. MBio 8.

760 29. Voss JE, Vaney MC, Duquerroy S, Vonrhein C, Girard-Blanc C, Crublet E,
761 Thompson A, Bricogne G, Rey FA. 2010. Glycoprotein organization of
762 Chikungunya virus particles revealed by X-ray crystallography. Nature 468:709-
763 12.

764 30. Li L, Jose J, Xiang Y, Kuhn RJ, Rossmann MG. 2010. Structural changes of
765 envelope proteins during alphavirus fusion. Nature 468:705-8.

766 31. Lescar J, Roussel A, Wien MW, Navaza J, Fuller SD, Wengler G, Rey FA. 2001.
767 The fusion glycoprotein shell of Semliki Forest virus: an icosahedral assembly
768 primed for fusogenic activation at endosomal pH. Cell 105:137-48.

769 32. Tsetsarkin KA, Chen R, Leal G, Forrester N, Higgs S, Huang J, Weaver SC.
770 2011. Chikungunya virus emergence is constrained in Asia by lineage-specific
771 adaptive landscapes. Proc Natl Acad Sci U S A 108:7872-7.

772 33. Tsetsarkin KA, Chen R, Yun R, Rossi SL, Plante KS, Guerbois M, Forrester N,
773 Perng GC, Sreekumar E, Leal G, Huang J, Mukhopadhyay S, Weaver SC. 2014.
774 Multi-peaked adaptive landscape for chikungunya virus evolution predicts
775 continued fitness optimization in Aedes albopictus mosquitoes. Nat Commun
776 5:4084.

777 34. Weaver SC, Winegar R, Manger ID, Forrester NL. 2012. Alphaviruses:
778 population genetics and determinants of emergence. Antiviral Res 94:242-57.

779 35. Pletnev SV, Zhang W, Mukhopadhyay S, Fisher BR, Hernandez R, Brown DT,
780 Baker TS, Rossmann MG, Kuhn RJ. 2001. Locations of carbohydrate sites on
781 alphavirus glycoproteins show that E1 forms an icosahedral scaffold. Cell
782 105:127-136.

783 36. Dunbar CA, Rayaprolu V, Wang JC, Brown CJ, Leishman E, Jones-Burrage S,
784 Trinidad JC, Bradshaw HB, Clemmer DE, Mukhopadhyay S, Jarrold MF. 2019.
785 Dissecting the Components of Sindbis Virus from Arthropod and Vertebrate
786 Hosts: Implications for Infectivity Differences. ACS Infect Dis 5:892-902.

787 37. Zandi R, Reguera D, Bruinsma RF, Gelbart WM, Rudnick J. 2004. Origin of
788 icosahedral symmetry in viruses. Proc Natl Acad Sci U S A 101:15556-60.

789 38. Basore K, Kim AS, Nelson CA, Zhang R, Smith BK, Uranga C, Vang L, Cheng M,
790 Gross ML, Smith J, Diamond MS, Fremont DH. 2019. Cryo-EM Structure of
791 Chikungunya Virus in Complex with the Mxra8 Receptor. Cell 177:1725-1737
792 e16.

793 39. Hasan SS, Sun C, Kim AS, Watanabe Y, Chen CL, Klose T, Buda G, Crispin M,
794 Diamond MS, Klimstra WB, Rossmann MG. 2018. Cryo-EM Structures of
795 Eastern Equine Encephalitis Virus Reveal Mechanisms of Virus Disassembly and
796 Antibody Neutralization. Cell Rep 25:3136-3147 e5.

797 40. Kostyuchenko VA, Jakana J, Liu X, Haddow AD, Aung M, Weaver SC, Chiu W,
798 Lok SM. 2011. The structure of barmah forest virus as revealed by cryo-electron
799 microscopy at a 6-angstrom resolution has detailed transmembrane protein
800 architecture and interactions. J Virol 85:9327-33.

801 41. Ribeiro-Filho HV, Coimbra LD, Cassago A, Rocha RPF, Guerra J, de Felicio R,
802 Carnieli CM, Leme L, Padilha AC, Paes Leme AF, Trivella DBB, Portugal RV,
803 Lopes-de-Oliveira PS, Marques RE. 2021. Cryo-EM structure of the mature and
804 infective Mayaro virus at 4.4 A resolution reveals features of arthritogenic
805 alphaviruses. Nat Commun 12:3038.

806 42. Chen L, Wang M, Zhu D, Sun Z, Ma J, Wang J, Kong L, Wang S, Liu Z, Wei L,
807 He Y, Wang J, Zhang X. 2018. Implication for alphavirus host-cell entry and
808 assembly indicated by a 3.5A resolution cryo-EM structure. Nat Commun 9:5326.

809 43. White J, Kielian M, Helenius A. 1983. Membrane fusion proteins of enveloped
810 animal viruses. Q Rev Biophys 16:151-95.

811 44. White J, Helenius A. 1980. pH-dependent fusion between the Semliki Forest
812 virus membrane and liposomes. Proc Natl Acad Sci U S A 77:3273-7.

813 45. Paroutis P, Touret N, Grinstein S. 2004. The pH of the secretory pathway:
814 measurement, determinants, and regulation. Physiology (Bethesda) 19:207-15.

815 46. Ashbrook AW, Burrack KS, Silva LA, Montgomery SA, Heise MT, Morrison TE,
816 Dermody TS. 2014. Residue 82 of the Chikungunya virus E2 attachment protein
817 modulates viral dissemination and arthritis in mice. J Virol 88:12180-92.

818 47. Jupille HJ, Medina-Rivera M, Hawman DW, Oko L, Morrison TE. 2013. A
819 tyrosine-to-histidine switch at position 18 of the Ross River virus E2 glycoprotein
820 is a determinant of virus fitness in disparate hosts. J Virol 87:5970-84.

821 48. Wang JC, Mukhopadhyay S, Zlotnick A. 2018. Geometric Defects and
822 Icosahedral Viruses. Viruses 10.

823 49. Scheres SH. 2016. Processing of Structurally Heterogeneous Cryo-EM Data in
824 RELION. Methods Enzymol 579:125-57.

825 50. Zivanov J, Nakane T, Forsberg BO, Kimanius D, Hagen WJ, Lindahl E, Scheres
826 SH. 2018. New tools for automated high-resolution cryo-EM structure
827 determination in RELION-3. Elife 7.

828 51. Pettersen EF, Goddard TD, Huang CC, Meng EC, Couch GS, Croll TI, Morris JH,
829 Ferrin TE. 2021. UCSF ChimeraX: Structure visualization for researchers,
830 educators, and developers. Protein Sci 30:70-82.

831

Fig 1

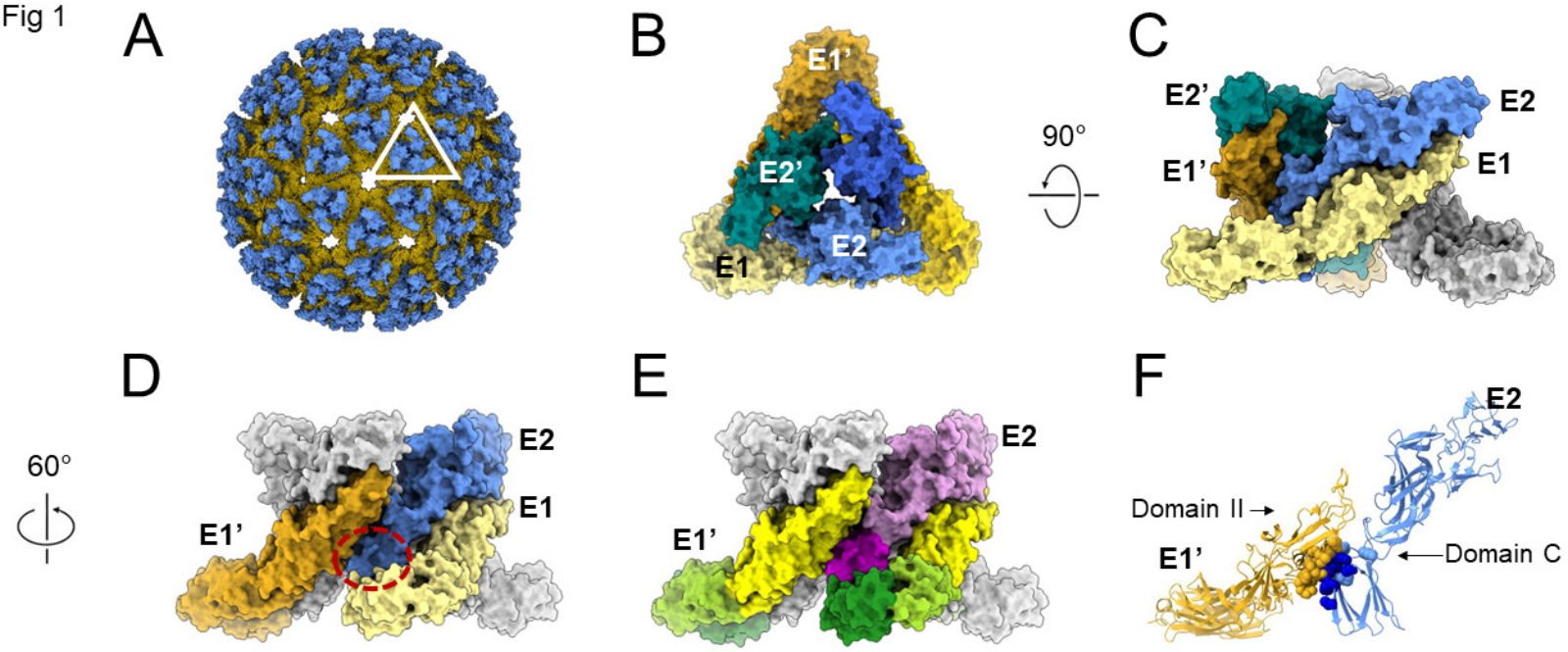

G

SINV	E2:	272	H	A	P	N	V	I	H	G	F	K	H	I	S	L	Q	L	D	288
CPB	E2:	272	R	N	P	T	V	T	H	G	F	K	H	I	S	L	L	L	Y	288
CHIKV	E2:	272	R	N	P	T	V	T	Y	G	K	N	Q	V	I	M	L	L	Y	288

Fig 2

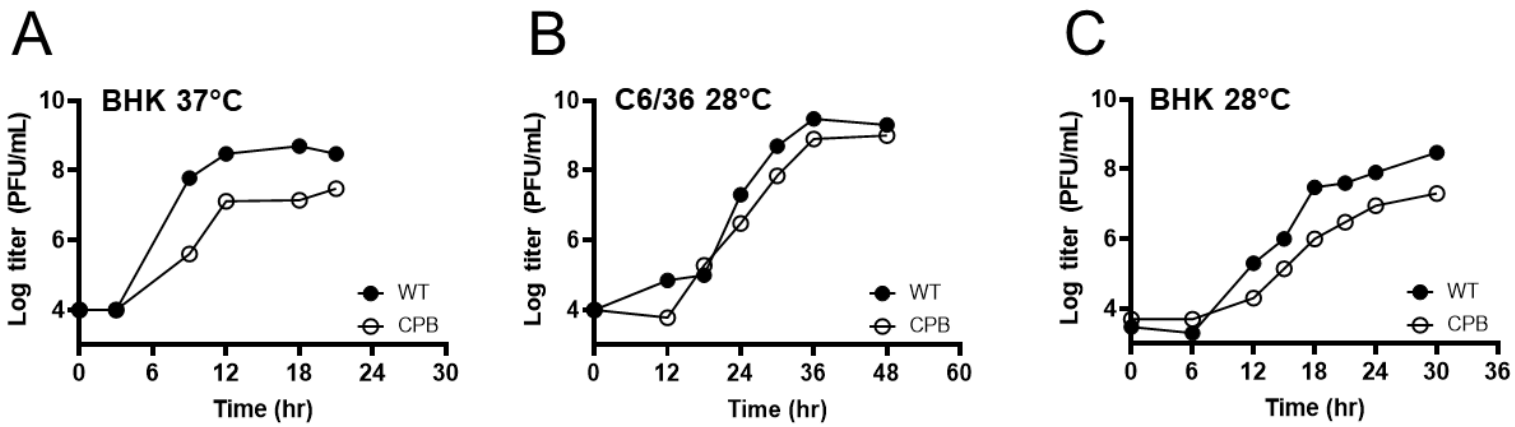
A
BHK 37°C
Log titer (PFU/mL)
Time (hr)
WT
CPB
B
C6/36 28°C
Log titer (PFU/mL)
Time (hr)
WT
CPB
C
BHK 28°C
Log titer (PFU/mL)
Time (hr)
WT
CPB

Fig 3

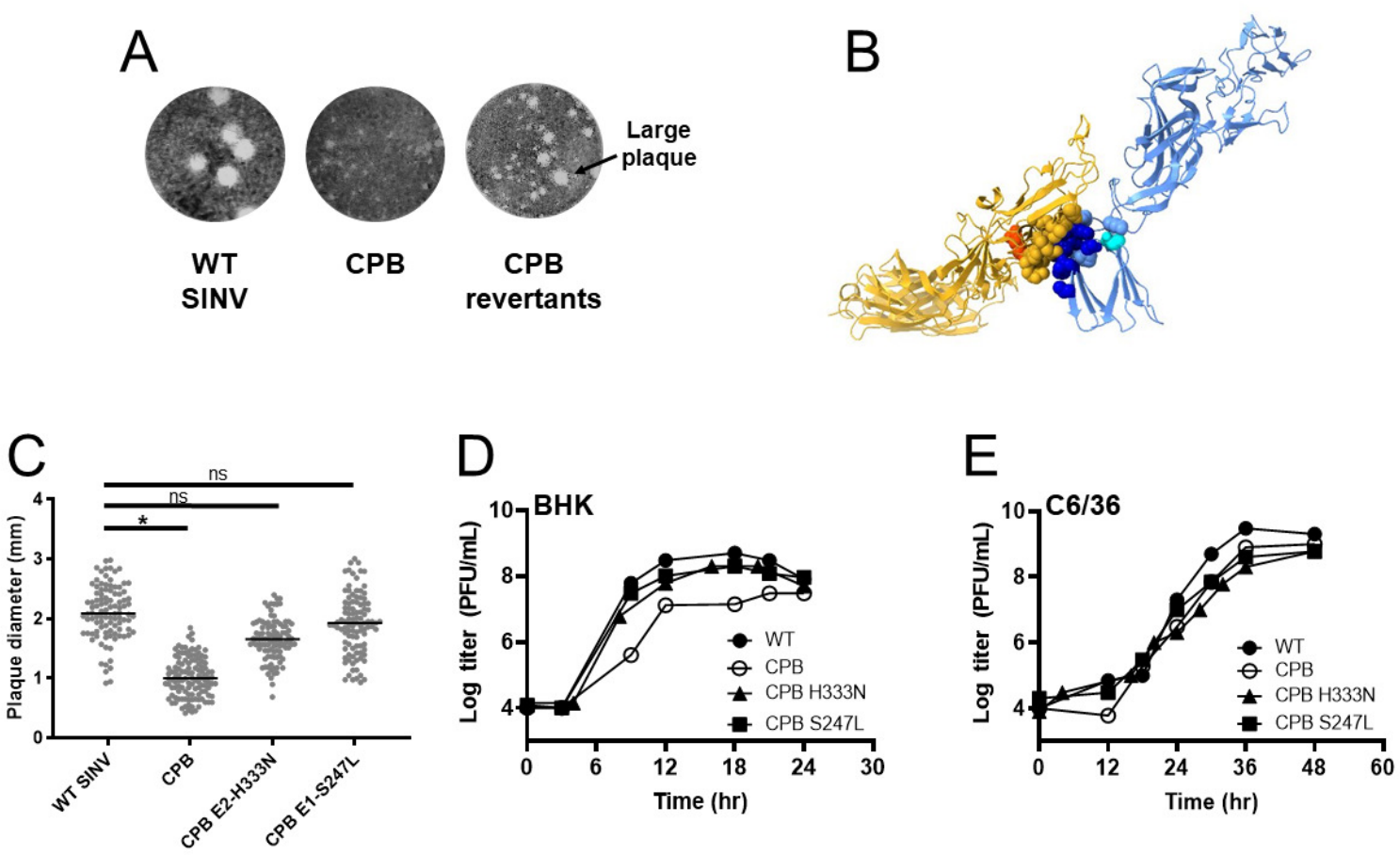
A
Large plaque
WT SINV
CPB
CPB revertants
B
C
ns
ns
*
Plaque diameter (mm)
WT SINV
CPB
CPB E2-H333N
CPB E1-S247L
D
BHK
Log titer (PFU/mL)
Time (hr)
WT
CPB
CPB H333N
CPB S247L
E
C6/36
Log titer (PFU/mL)
Time (hr)
WT
CPB
CPB H333N
CPB S247L

Fig 4
A, B

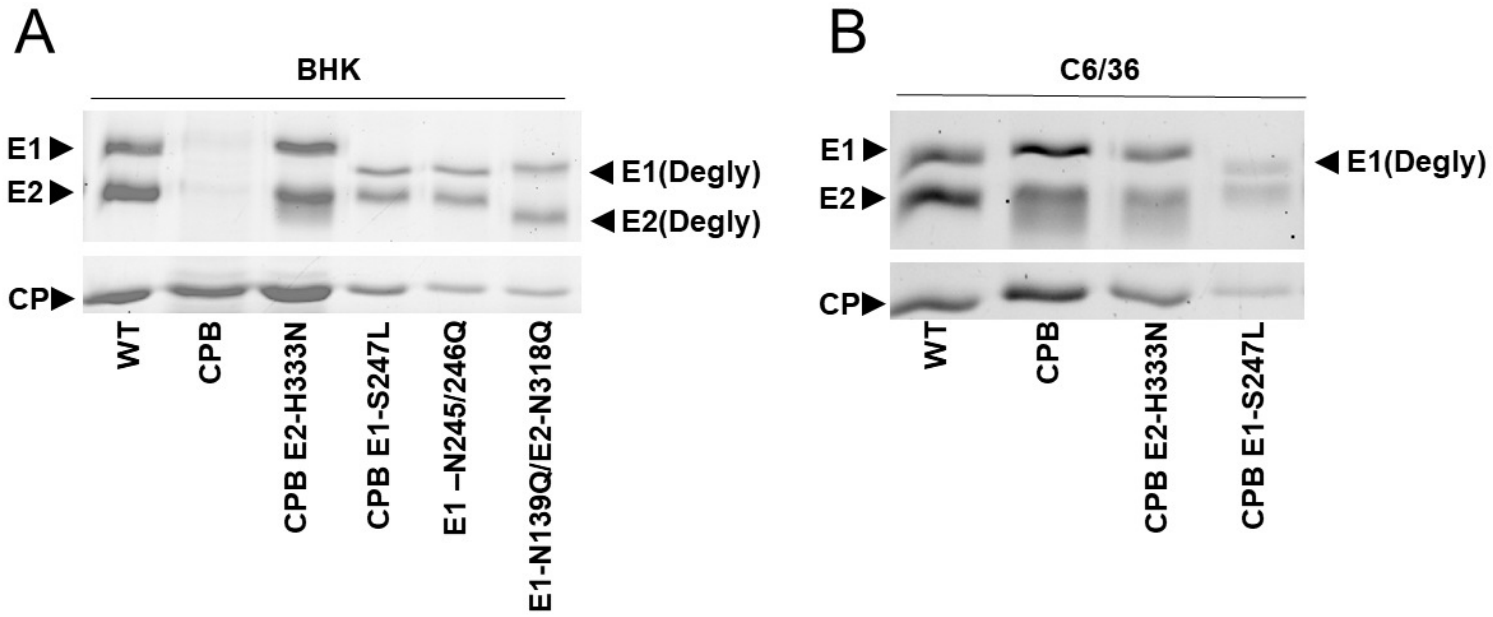
A
BHK
E1
E2
CP
E1(Degly)
E2(Degly)
WT
CPB
CPB E2-H333N
CPB E1-S247L
E1 –N245/246Q
E1-N139Q/E2-N318Q
B
C6/36
E1
E2
CP
E1(Degly)
WT
CPB
CPB E2-H333N
CPB E1-S247L

Fig 4
C, D

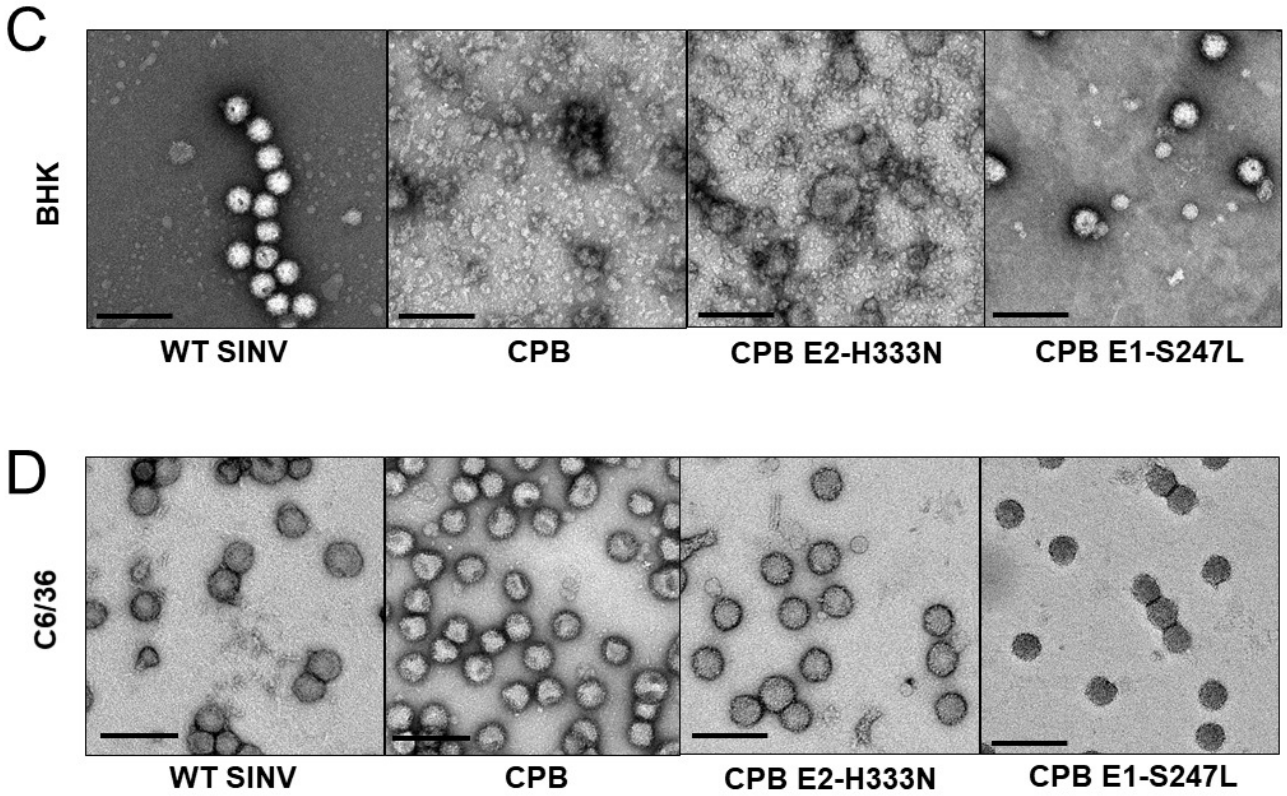
C
BHK
WT SINV
CPB
CPB E2-H333N
CPB E1-S247L
D
C6/36
WT SINV
CPB
CPB E2-H333N
CPB E1-S247L

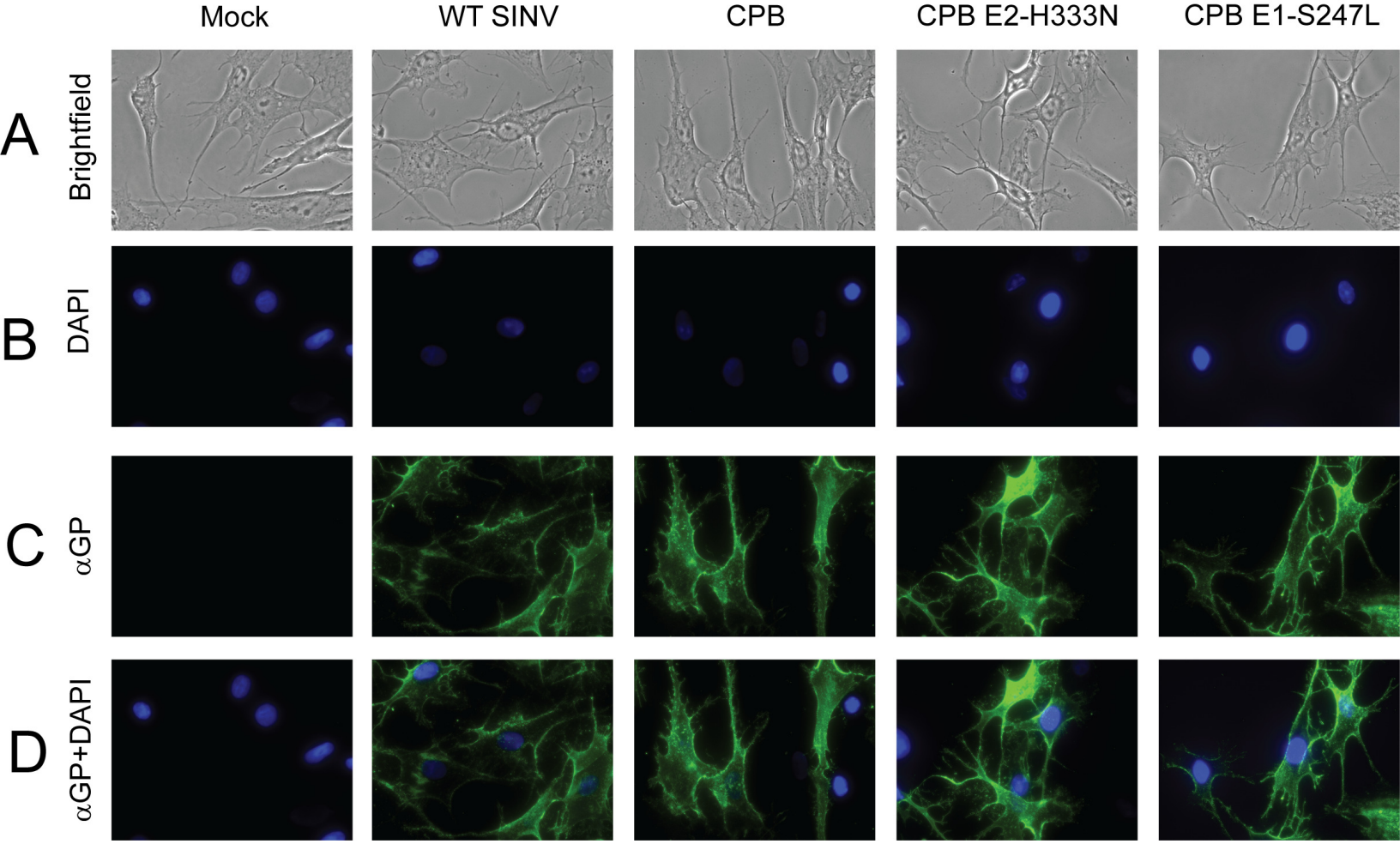
Mock
WT SINV
CPB
CPB E2-H333N
CPB E1-S247L
A
Brightfield
B
DAPI
C
αGP
D
αGP+DAPI

Fig 6, A-F

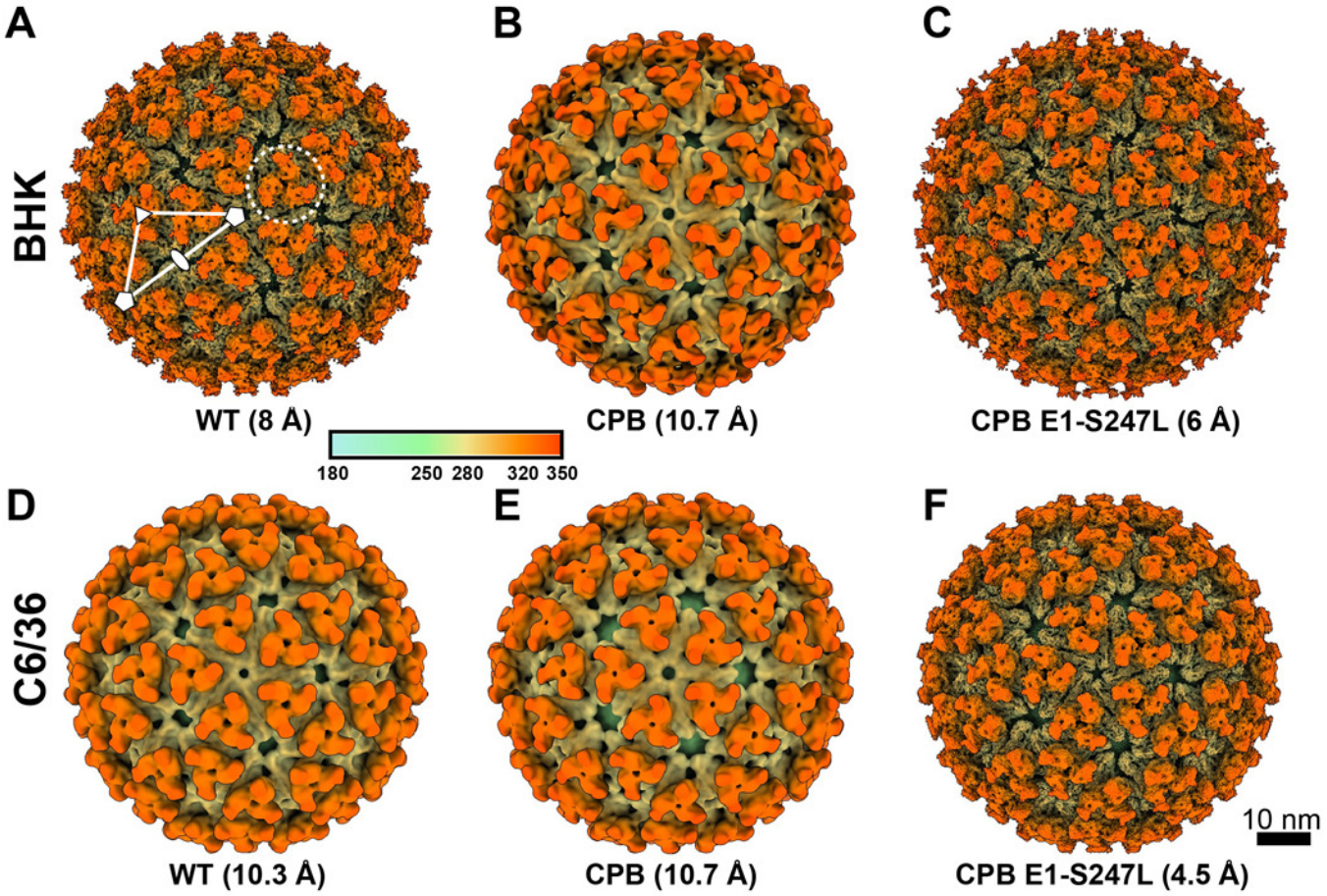
A
B
C
BHK
WT (8 Å)
CPB (10.7 Å)
CPB E1-S247L (6 Å)
180
250 280
320 350
D
E
F
C6/36
WT (10.3 Å)
CPB (10.7 Å)
CPB E1-S247L (4.5 Å)
10 nm

Fig 6,
G-L

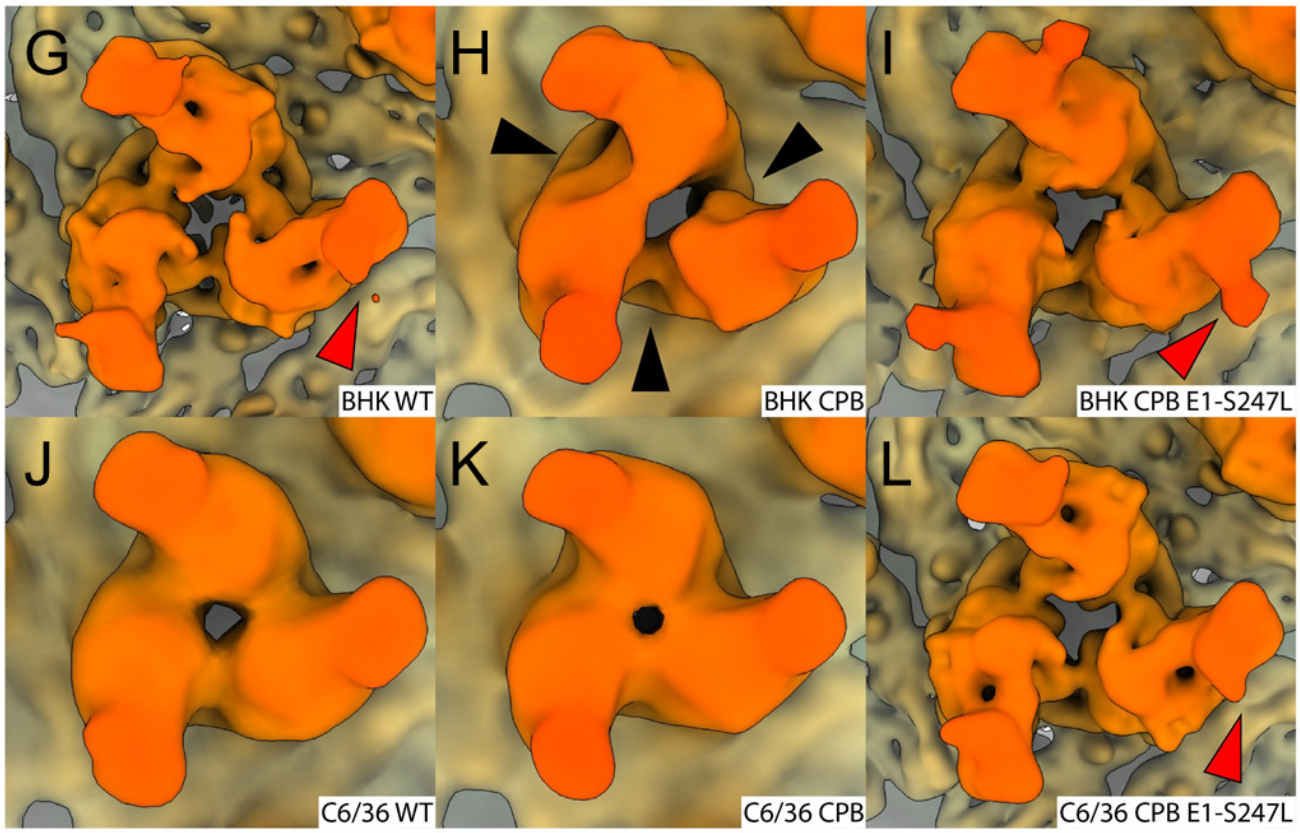
G
BHK WT
H
BHK CPB
I
BHK CPB E1-S247L
J
C6/36 WT
K
C6/36 CPB
L
C6/36 CPB E1-S247L

Table 1: Location of glycosylation sites

Virus	Protein	Glycosylation site
SINV	E2	N196
SINV	E2	N318
SINV	E1	N139
SINV	E1	N245
CHIKV	E2	N263
CHIKV	E2	N345
CHIKV	E1	N141

Reconstruction data	WT SINV (BHK)	CPB (BHK)	CPB E1-S247L (BHK)	WT SINV (C6/36)	CPB (C6/36)	CPB E1-S247L (C6/36)
Data collection information						
Electron microscope	TFS Titan Krios	TFS Titan Krios	TFS Titan Krios	JEOL 3200FS	TFS Titan Krios	TFS Titan Krios
Operation voltage (kV)	300	300	300	300	300	300
Electron detector	Gatan K3	Gatan K3	Gatan K3	DE-12	Gatan K3	Gatan K3
Energy filter (slit width in eV)	20	20	20	20	20	20
Data collection mode	Counting	Super-resolution counting	Counting	Integrated	Counting	Counting
Nominal magnification	105,000x	64,000x	64,000x	80,000x	64,000x	64,000x
Pixel size in 3D map (Å) (Pixel size in the censor)	1.68 (0.84)	2.72 (0.68)	1.36 (1.36)	1.9 (1.9)	2.72 (1.36)	1.36 (1.36)
Total accumulated dose (e^-/ $Å^2$)	30	30	30	30	30	30
Data process statistics						
Box size (pixel)	500	300	600	440	300	600
Number of particles	9037	15956	16133	7102	63509	65053
CTF estimation	CTFFIND4	CTFFIND4	CTFFIND4	CTFFIND4	CTFFIND4	CTFFIND4
Data processing software	RELION 3.1	RELION 3.1	RELION 3.1	RELION 3.1	RELION 3.1	RELION 3.1
Symmetry imposition	I2	I2	I2	I2	I2	I2
B-factor applied ($Å^2$)	-545.7	N/A	-311.4	-297.3	N/A	-237.3
Final resolution (Å)	8	10.7	5.9	10.3	10.7	4.5